Department of Physics

CAPP

Maintaining quality factor of superconducting $YBa_2Cu_3O_{7-x}$ microwave cavity in a high magnetic field

Danho Ahn,[1,2] Ohjoon Kwon,[1] Sung Woo Youn,[1] Wonjun Jang,[3] Jhinhwan Lee,[4] Woohyun Chung,[1] Dojun Youm,[2] Yannis K. Semertzidis.[1,2]

[1]Center for Axion and Precision Physics, Institute of Basic Science, Daejeon 34141, Repulic of Korea

[2]Department of Physics, Korea Advanced Institute of Science and Technology, Daejeon 34141, Republic of Korea

[3]Center for Quantum Nanoscience, Institute of Basic Science, Seoul 33760, Republic of Korea

[3]Center for Artificial Low Dimensional Electronic Systems, Institute of Basic Science, Seoul 33760, Republic of Korea

Superconducting Radio-Frequency Cavity

SCIENTIFIC REPORTS

OPEN

Tunable Superconducting Cavity using Superconducting Quantum Interference Device Metamaterials

Received: 8 November 2018
Accepted: 21 February 2019
Published online: 15 March 2019

Samuel Kim[1,2], David Shrekenhamer[1], Kyle McElroy[1], Andrew Strikwerda[1] & Jacob Alldredge[1]

Here we consider a tunable superconducting cavity that can be used either as a tunable coupler to a qubit inside the cavity or as a tunable low noise, low temperature, RF filter. Our design consists of an array of radio-frequency superconducting quantum interference devices (rf SQUIDs) inside a superconducting cavity. This forms a tunable metamaterial structure which couples to the cavity through its magnetic plasma frequency. By tuning the resonant frequency of the metamaterial through an applied magnetic flux, one can tune the cavity mode profile. This allows us to detune the cavity initially centered at 5.593 GHz by over 200 MHz. The maximum quality factor approaches that of the empty cavity, which is 4.5×10^6. The metamaterial electromagnetic response is controlled via a low-frequency or dc magnetic flux bias, and we present a control line architecture that is capable of applying sufficient magnetic flux bias with minimal parasitic coupling. Together this design allows for an *in-situ* tunable cavity which enables low-temperature quantum control applications.

Supercond. Sci. Technol. **30** (2017) 053003 (23pp) https://doi.org/10.1088/1361-6668/aa6376

Topical Review

50 years of success for SRF accelerators—a review

Hasan Padamsee

Cornell University, Ithaca, NY 14850, United States of America

Received 7 August 2016, revised 17 November 2016
Accepted for publication 28 February 2017
Published 18 April 2017

CrossMark

Abstract
The past five decades have seen many successes in superconducting radio-frequency (SRF) enabling a variety of accelerators. These successes are the result of steady progress in understanding the science behind the performance limitations, and in developing effective countermeasures to advance key performance aspects. SRF technology has developed in parallel to bring major accelerators to reality for a wide variety of fields from high energy physics, nuclear physics, and nuclear astro-physics to materials science.

Keywords: accelerators, niobium, gradients, quality-factor

(Some figures may appear in colour only in the online journal)

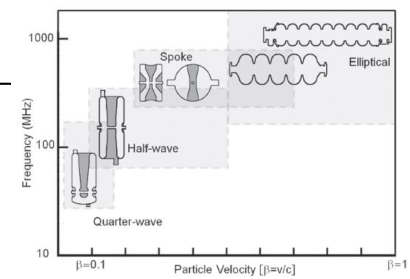

Figure 1. Superconducting cavities spanning the full range of β [9]. Reproduced with permission from [12]. Copyright © 2013, CCC Republication.

Supercond. Sci. Technol. **30** (2017) 035009 J Wosik *et al*

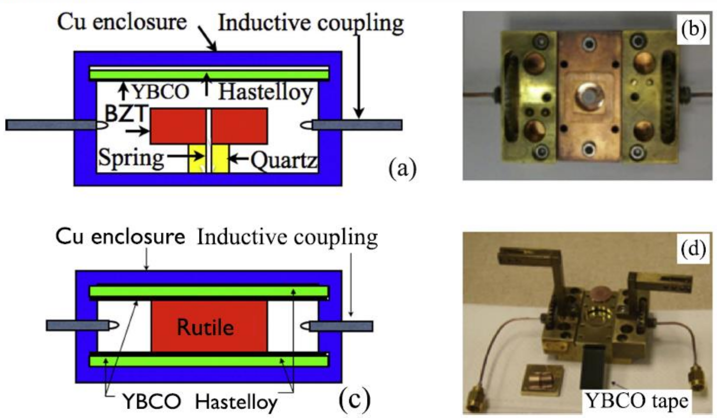

Figure 2. Schematic representation of (a) $TE_{01\delta}$ mode 13 GHz BZT SiPDR and (b) TE_{011} mode 9.4 GHz rutile RDR, designed to accommodate 12 mm wide tapes, are shown. SiPDR and RDR pictures are presented in (c) and (d), respectively.

SRF in High Magnetic Field

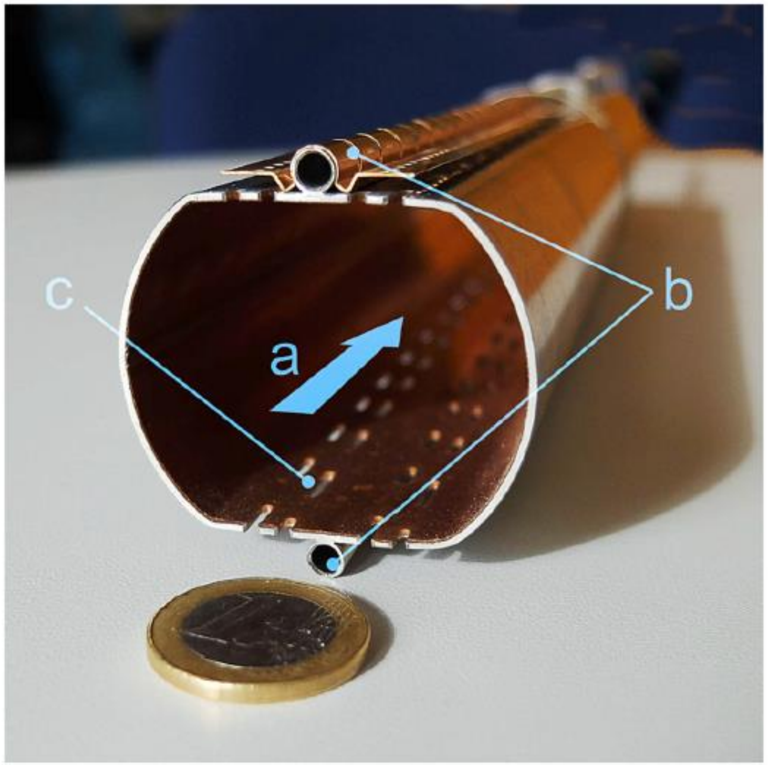

Figure 1. Photograph of the LHC beam screen. The proton beam moves along the axis indicated by the arrow (a). The tubes on top and at the bottom (b) are cooling channels for gaseous helium, and the slots (c) allow any desorbed gases to escape and to be cryopumped onto the surface of the cold bore of the surrounding magnet.

S. Calatroni *et al*, *Supercond. Sci. Technol.* **30** 075002 (2017).

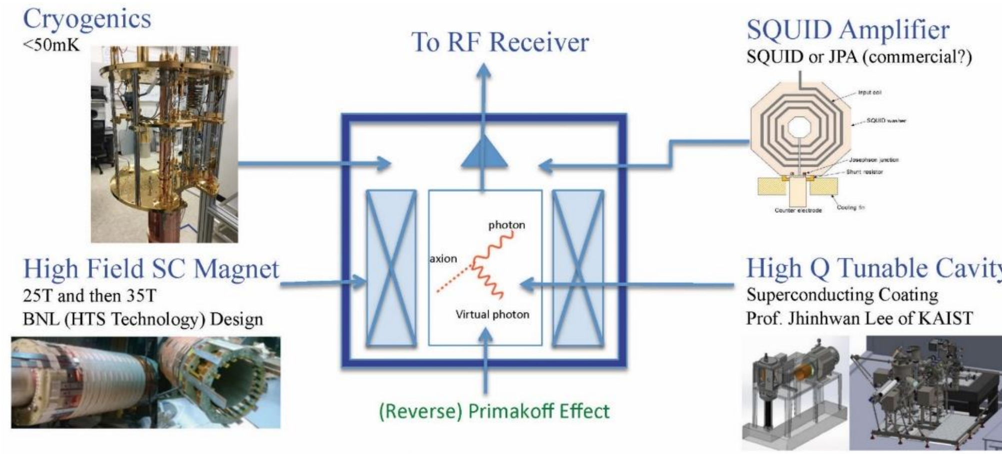

$$P_{\alpha\to\gamma\gamma} = g^2{}_{\alpha\gamma\gamma}\frac{\rho_a}{m_a}B^2 V C_{mnp} min(Q_L, Q_a)$$

$$SNR = \frac{P_{signal}}{P_{noise}} = \frac{P_{\alpha\to\gamma\gamma}}{k_B T_{sys}}\sqrt{\frac{t_{int}}{\Delta f_a}}$$

$$\frac{df}{dt} \propto \frac{B^4 V^2 C^2 min(Q_L, Q_A)}{T_{sys}{}^2}$$

Vortices in Superconducting Surface

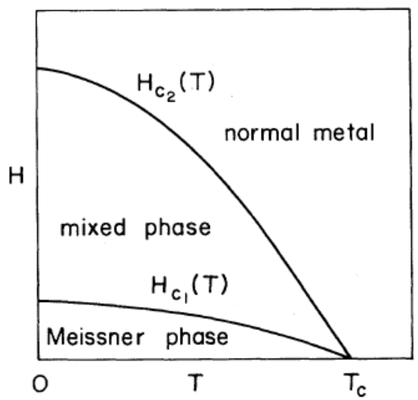

FIG. 1. Mean-field phase diagram comprising a normal-metallic phase at high fields and temperatures, separated by the upper critical-field line $H_{c_2}(T)$ from the mixed or Shubnikov phase, which in turn is separated by the lower critical-field line $H_{c_1}(T)$ from the Meissner-Ochsenfeld phase at low temperatures and fields.

G. Blatter et al, 1994 *Rev. Mod. Phys.* **66** 1125

$$\frac{\rho_{vortex}}{\rho_{normal}} \approx \frac{B}{H_{c2}}$$

Resistivity from un-pinned vortices

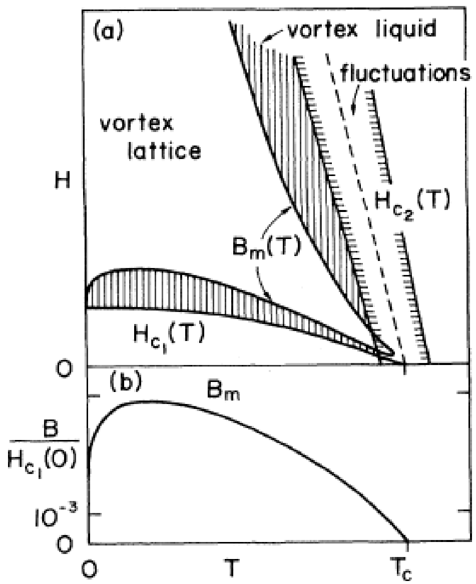

FIG. 2. Phenomenological phase diagram for the anisotropic high-temperature superconductors [parameters for YBCO, $H_{c_1}(0) \approx 730$ G, $H_{c_2}(0) \approx 230$ T, values extrapolated linearly to zero, see also Sec. II.C]: (a) The Abrikosov vortex lattice is melted over a substantial part of the phase diagram. The vortex lattice can melt with increasing temperature (thermal fluctuations) or with decreasing field (exponentially vanishing shear modulus), leading to a reentrant behavior of the melting line $B_m(T)$. The thermodynamic phase transition is shifted to the melting line $B_m(T)$, with the upper critical-field line $H_{c_2}(T)$ marking only a crossover line where the modulus of the order parameter increases rapidly. The regime of large critical fluctuations where the description in terms of vortex (phase) fluctuations breaks down and amplitude fluctuations become important is confined to a rather narrow (~ 1 K wide) region close to $H_{c_2}(T)$. The drawing is not to scale, but emphasizes the main structures appearing in the phase diagram. (b) Shape of the melting line $B_m(T)$ for YBCO with parameters $\xi_{BCS} \approx 16$ Å, $\lambda_L \approx 1400$ Å, and an anisotropy parameter $\varepsilon^2 = M/m \approx 1/25$; drawing is to scale. Note that the extent of the dilute vortex-liquid phase along the field axis is only of the order of a few gauss.

G. Blatter et al, 1994 *Rev. Mod. Phys.* **66** 1125

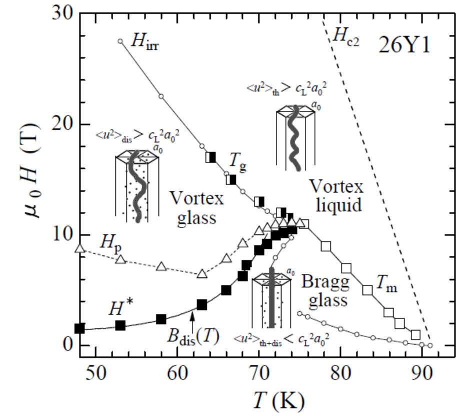

Figure 7. The vortex-matter phase diagram in untwinned $YBa_2Cu_3O_y$. The transition lines $T_m(H)$, $T_g(H)$, and $H^*(T)$ terminate at the critical point and divide into three different phases of the vortex liquid, the vortex glass, and the Bragg glass. The full curve is a fit to the field-driven transition line $B_{dis}(T)$.

Terukazu Nishizaki and Norio Kobayashi 2000 *Supercond. Sci. Technol.* **13** 1

Niobium Titanium Film

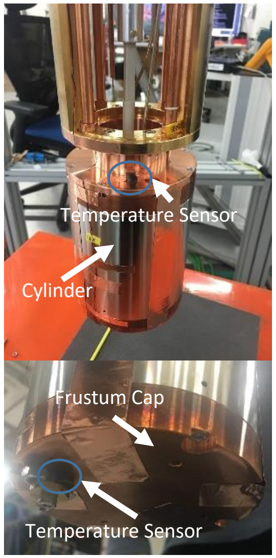

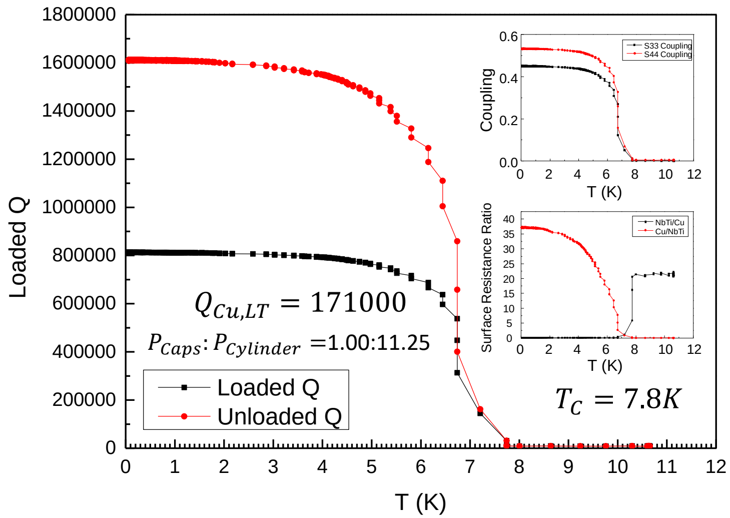

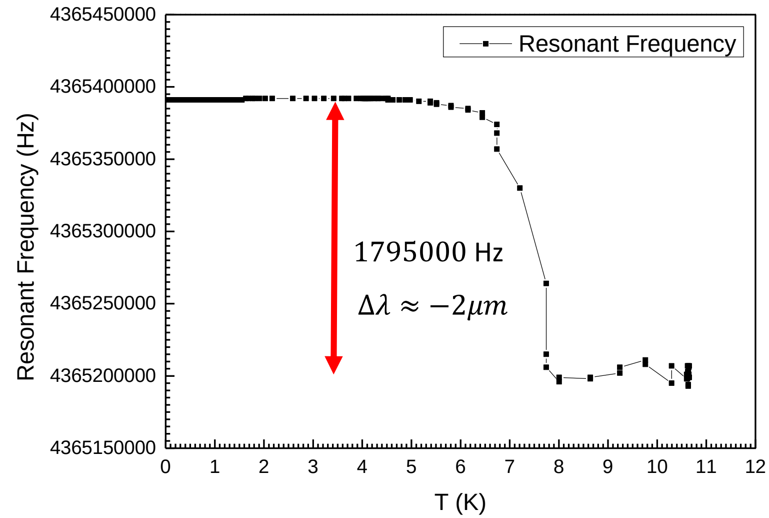

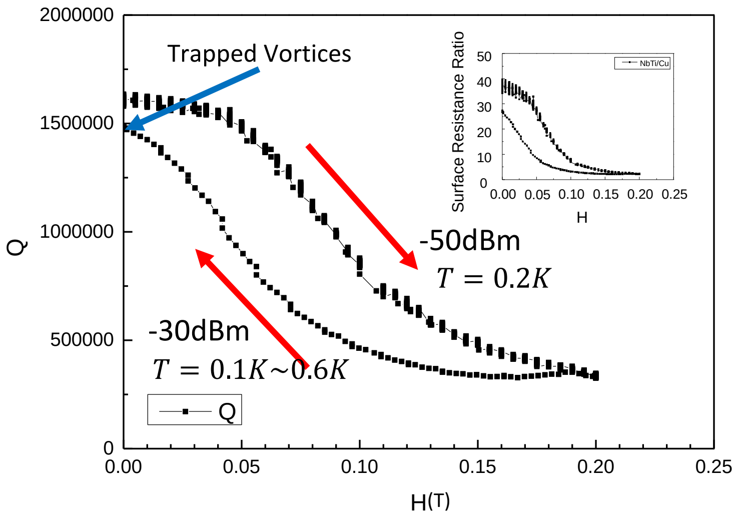

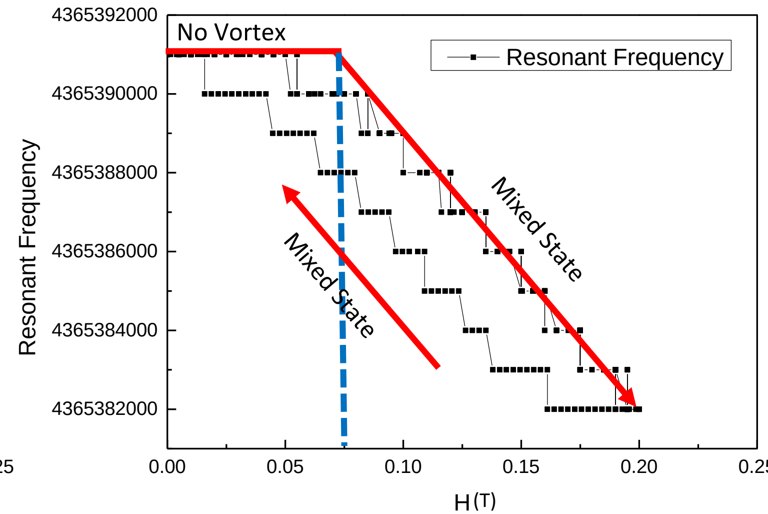

Why YBCO tapes?

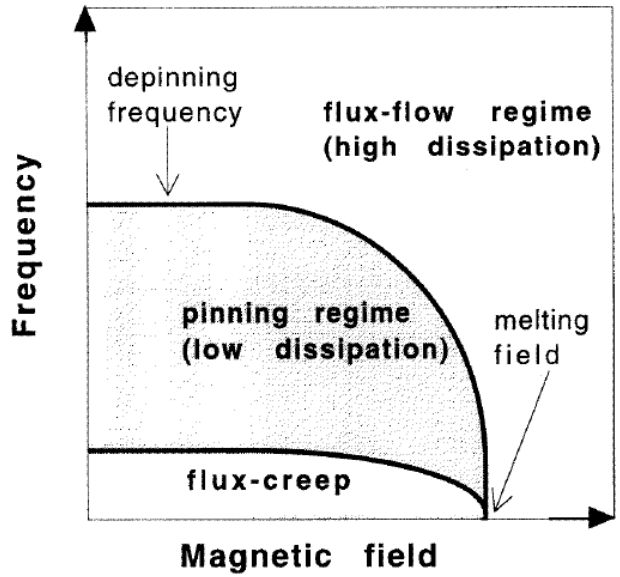

Figure 6. A schematic field–frequency diagram. In the pinning regime the vortex resistivity is primarily inductive and is determined by pinning. In the flux-flow regime the vortex resistivity is primarily resistive and is determined by viscosity, irrespective of whether vortices are pinned or unpinned. In the flux-creep (TAFF) regime the vortex resistivity is primarily resistive, although it is much smaller than in the flux-flow regime. The lines separating different regimes of the vortex dissipation are determined by the condition $\mathrm{Im}(\rho_v) = \mathrm{Re}(\rho_v)$ and do not necessarily coincide with phase transitions.

M. Golosovsky, M. Tsindlekht, D. Dvidov, *Supercond. Sci. Technol.* **9** 1 (1996).

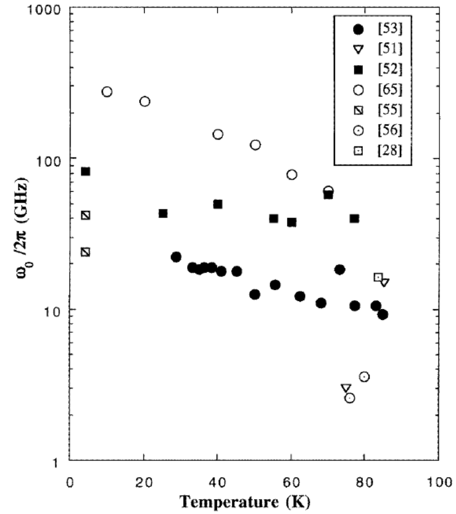

Figure 13. Temperature dependence of the depinning frequency.

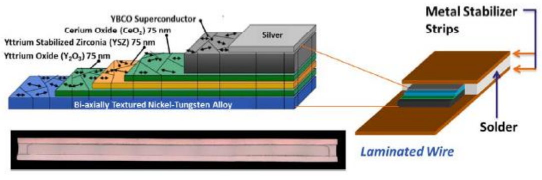

Fig. 1. Schematic illustration of the architecture of AMSC's insert and laminated wire architectures. A micrograph of an actual Amperium wire cross-section is shown in the bottom left.

M. W. Rupich *et al*, *IEEE Trans. Appl. Supercond.* **23** 6601205 (2013).

Epitaxial $YBa_2Cu_3O_7$ on Biaxially Textured Nickel (001): An Approach to Superconducting Tapes with High Critical Current Density

David P. Norton, Amit Goyal, John D. Budai, David K. Christen, Donald M. Kroeger, Eliot D. Specht, Qing He, Bernd Saffian, M. Paranthaman, Charles E. Klabunde, Dominic F. Lee, Brian C. Sales, Fred A. List

In-plane–aligned, c axis–oriented $YBa_2Cu_3O_7$ (YBCO) films with superconducting critical current densities J_c as high as 700,000 amperes per square centimeter at 77 kelvin have been grown on thermomechanically rolled-textured nickel (001) tapes by pulsed-laser deposition. Epitaxial growth of oxide buffer layers directly on biaxially textured nickel, formed by recrystallization of cold-rolled pure nickel, made possible the growth of YBCO films 1.5 micrometers thick with superconducting properties that are comparable to those observed for epitaxial films on single-crystal oxide substrates. This result represents a viable approach for the production of long superconducting tapes for high-current, high-field applications at 77 kelvin.

D. P. Norton *et al*, *Science* **274** 755 (1996).

Cavity Design and Comsol Simulation

- Electric Field (red arrows, colored 3D plot)
- Magnetic field (yellow arrows)
- 6.85 GHz

- Surface Current (blue arrows, colored surface plot)
- 6.85 GHz

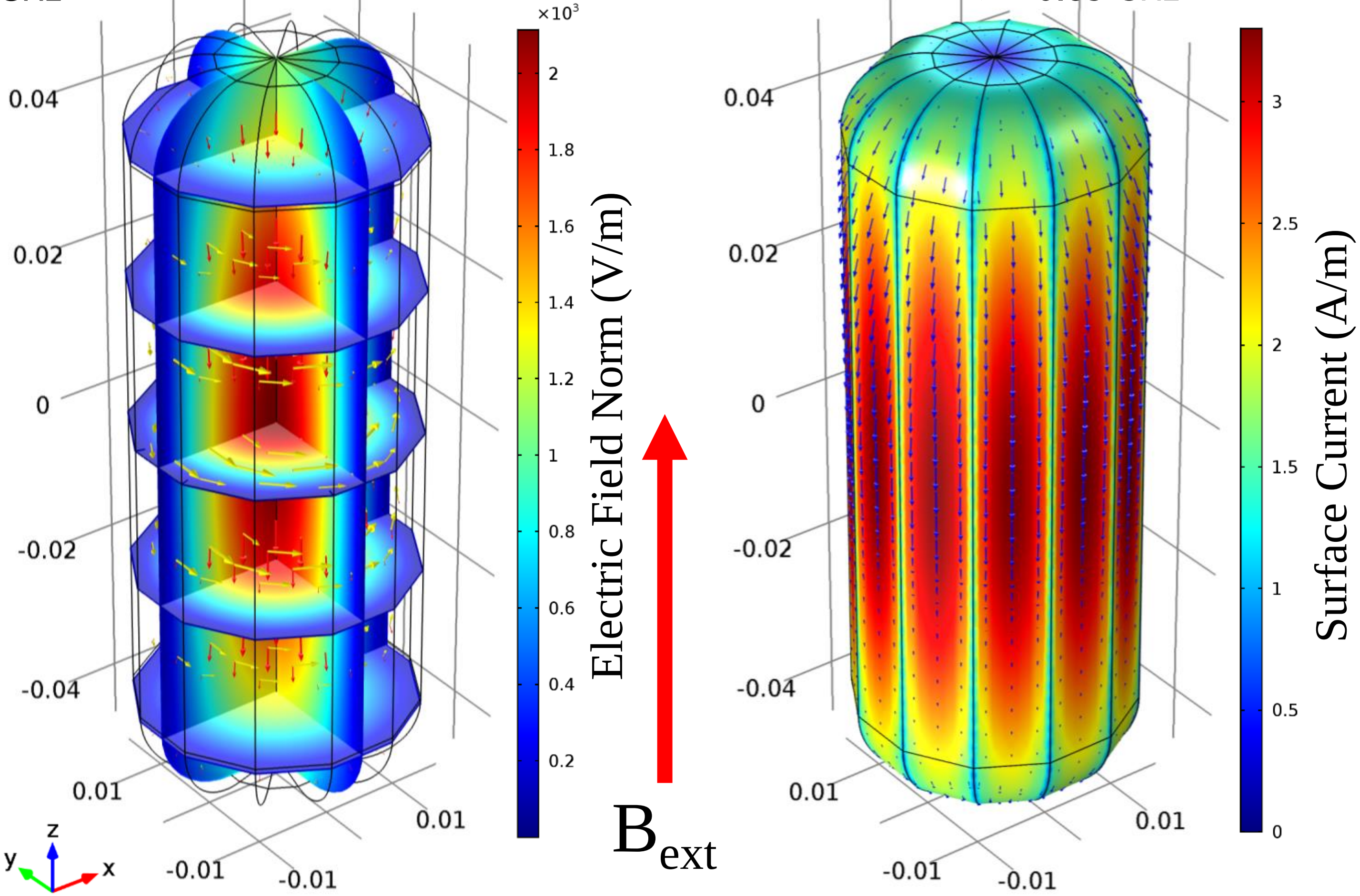

YBCO Tape Attachment

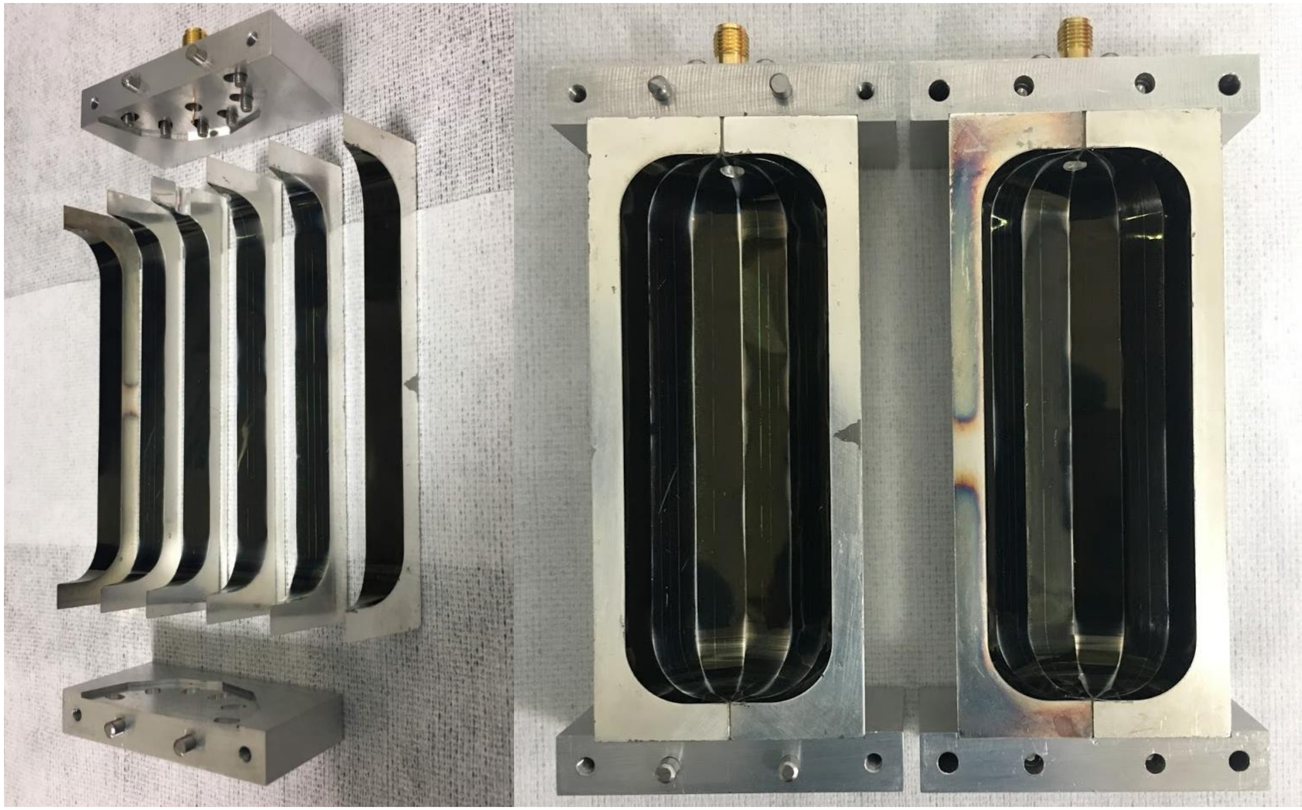

- Attach YBCO tape on the cavity inner surface with epoxy.
- Cut edges of the YBCO tapes exposed on the side.
- Remove protective layer.
- Sputter silver on the side of the tape.

RF Measurement in Cryo-cooler

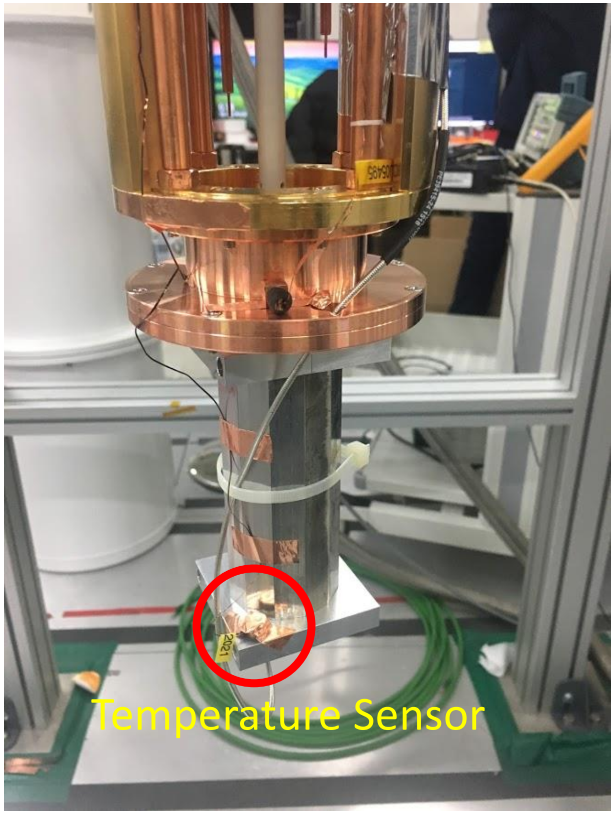

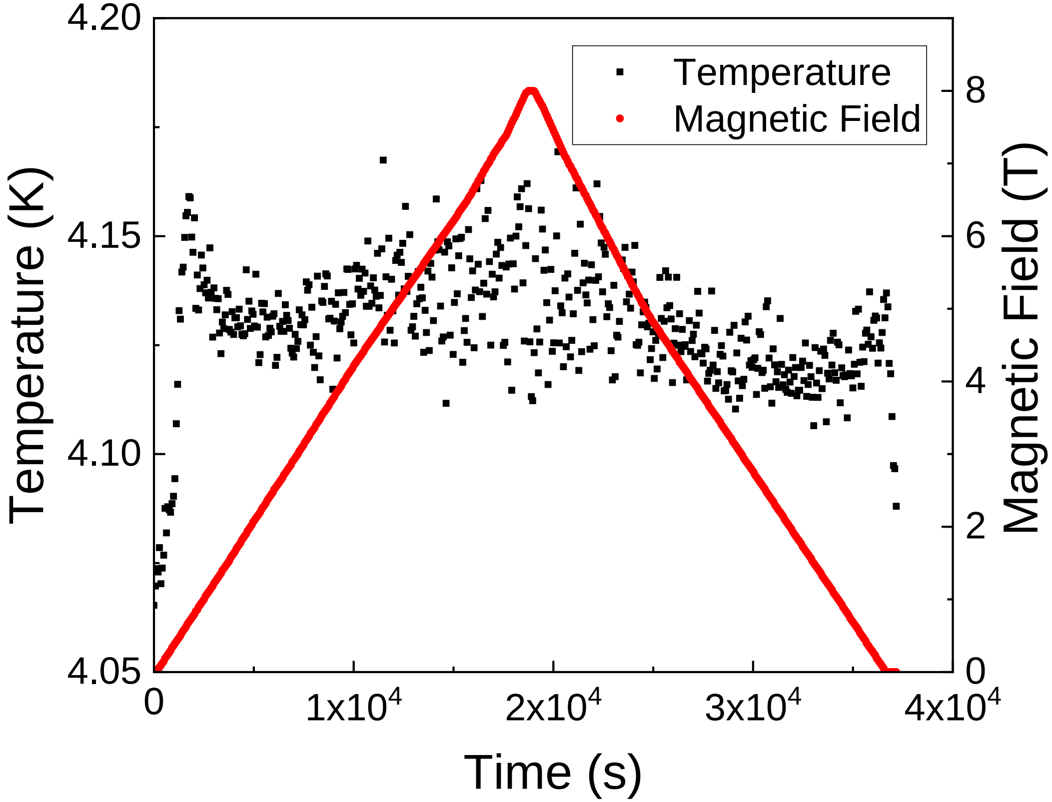

- A temperature sensor had been attached at the bottom of the cavity.
- For the temperature measurement the temperature had been varied from 300 K to 4.06 K.
- For the magnetic field measurement the temperature had been varied from 4.06 K to 4.15 K.

Data Aquisition

$$Q_R = Q_L(1 + \beta_1 + \beta_2),\ \beta_i = \frac{1 - S_{ii}}{1 + S_{ii}} \text{ (undercoupled case)}$$

$$\frac{1}{Q} = \sum \frac{P_{YBCO\ film} + P_{etc}}{\omega U_{tot}}$$

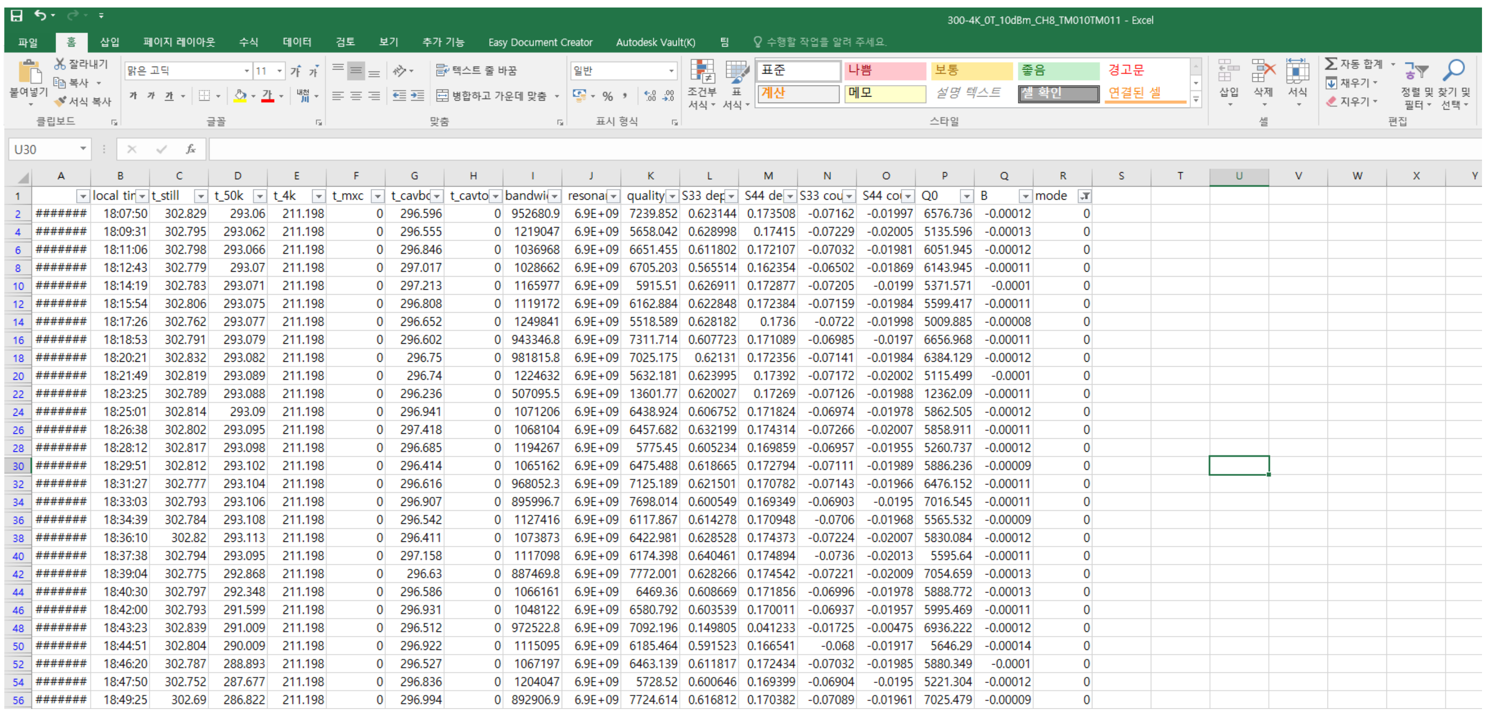

	A	local tir	t_still	t_50k	t_4k	t_mxc	t_cavbc	t_cavto	bandwi	resona	quality	S33 dep	S44 de	S33 cou	S44 co	Q0	B	mode
2	#######	18:07:50	302.829	293.06	211.198	0	296.596	0	952680.9	6.9E+09	7239.852	0.623144	0.173508	-0.07162	-0.01997	6576.736	-0.00012	0
4	#######	18:09:31	302.795	293.062	211.198	0	296.555	0	1219047	6.9E+09	5658.042	0.628998	0.17415	-0.07229	-0.02005	5135.596	-0.00013	0
6	#######	18:11:06	302.798	293.066	211.198	0	296.846	0	1036968	6.9E+09	6651.455	0.611802	0.172107	-0.07032	-0.01981	6051.945	-0.00012	0
8	#######	18:12:43	302.779	293.07	211.198	0	297.017	0	1028662	6.9E+09	6705.203	0.565514	0.162354	-0.06502	-0.01869	6143.945	-0.00011	0
10	#######	18:14:19	302.783	293.071	211.198	0	297.213	0	1165977	6.9E+09	5915.51	0.626911	0.172877	-0.07205	-0.0199	5371.571	-0.0001	0
12	#######	18:15:54	302.806	293.075	211.198	0	296.808	0	1119172	6.9E+09	6162.884	0.622848	0.172384	-0.07159	-0.01984	5599.417	-0.00011	0
14	#######	18:17:26	302.762	293.077	211.198	0	296.652	0	1249841	6.9E+09	5518.589	0.628182	0.1736	-0.0722	-0.01998	5009.885	-0.00008	0
16	#######	18:18:53	302.791	293.079	211.198	0	296.602	0	943346.8	6.9E+09	7311.714	0.607723	0.171089	-0.06985	-0.0197	6656.968	-0.00011	0
18	#######	18:20:21	302.832	293.082	211.198	0	296.75	0	981815.8	6.9E+09	7025.175	0.62131	0.172356	-0.07141	-0.01984	6384.129	-0.00012	0
20	#######	18:21:49	302.819	293.089	211.198	0	296.74	0	1224632	6.9E+09	5632.181	0.623995	0.17392	-0.07172	-0.02002	5115.499	-0.0001	0
22	#######	18:23:25	302.789	293.088	211.198	0	296.236	0	507095.5	6.9E+09	13601.77	0.620027	0.17269	-0.07126	-0.01988	12362.09	-0.00011	0
24	#######	18:25:01	302.814	293.09	211.198	0	296.941	0	1071206	6.9E+09	6438.924	0.606752	0.171824	-0.06974	-0.01978	5862.505	-0.00012	0
26	#######	18:26:38	302.802	293.095	211.198	0	297.418	0	1068104	6.9E+09	6457.682	0.632199	0.174314	-0.07266	-0.02007	5858.911	-0.00011	0
28	#######	18:28:12	302.817	293.098	211.198	0	296.685	0	1194267	6.9E+09	5775.45	0.605234	0.169859	-0.06957	-0.01955	5260.737	-0.00012	0
30	#######	18:29:51	302.812	293.102	211.198	0	296.414	0	1065162	6.9E+09	6475.488	0.618665	0.172794	-0.07111	-0.01989	5886.236	-0.00009	0
32	#######	18:31:27	302.777	293.104	211.198	0	296.616	0	968052.3	6.9E+09	7125.189	0.621501	0.170782	-0.07143	-0.01966	6476.152	-0.00011	0
34	#######	18:33:03	302.793	293.106	211.198	0	296.907	0	895996.7	6.9E+09	7698.014	0.600549	0.169349	-0.06903	-0.0195	7016.545	-0.00011	0
36	#######	18:34:39	302.784	293.108	211.198	0	296.542	0	1127416	6.9E+09	6117.867	0.614278	0.170948	-0.0706	-0.01968	5565.532	-0.00009	0
38	#######	18:36:10	302.82	293.113	211.198	0	296.411	0	1073873	6.9E+09	6422.981	0.628528	0.174373	-0.07224	-0.02007	5830.084	-0.00012	0
40	#######	18:37:38	302.794	293.095	211.198	0	297.158	0	1117098	6.9E+09	6174.398	0.640461	0.174894	-0.0736	-0.02013	5595.64	-0.00011	0
42	#######	18:39:04	302.775	292.868	211.198	0	296.63	0	887469.8	6.9E+09	7772.001	0.628266	0.174542	-0.07221	-0.02009	7054.659	-0.00013	0
44	#######	18:40:30	302.797	292.348	211.198	0	296.586	0	1066161	6.9E+09	6469.36	0.608669	0.171856	-0.06996	-0.01978	5888.772	-0.00013	0
46	#######	18:42:00	302.793	291.599	211.198	0	296.931	0	1048122	6.9E+09	6580.792	0.603539	0.170011	-0.06937	-0.01957	5995.469	-0.00011	0
48	#######	18:43:23	302.839	291.009	211.198	0	296.512	0	972522.8	6.9E+09	7092.196	0.149805	0.041233	-0.01725	-0.00475	6936.222	-0.00012	0
50	#######	18:44:51	302.804	290.009	211.198	0	296.922	0	1115095	6.9E+09	6185.464	0.591523	0.166541	-0.068	-0.01917	5646.29	-0.00014	0
52	#######	18:46:20	302.787	288.893	211.198	0	296.527	0	1067197	6.9E+09	6463.139	0.611817	0.172434	-0.07032	-0.01985	5880.349	-0.0001	0
54	#######	18:47:50	302.752	287.677	211.198	0	296.836	0	1204047	6.9E+09	5728.52	0.600646	0.169399	-0.06904	-0.0195	5221.304	-0.00012	0
56	#######	18:49:25	302.69	286.822	211.198	0	296.994	0	892906.9	6.9E+09	7724.614	0.616812	0.170382	-0.07089	-0.01961	7025.479	-0.00009	0

Temperature Measurement Result

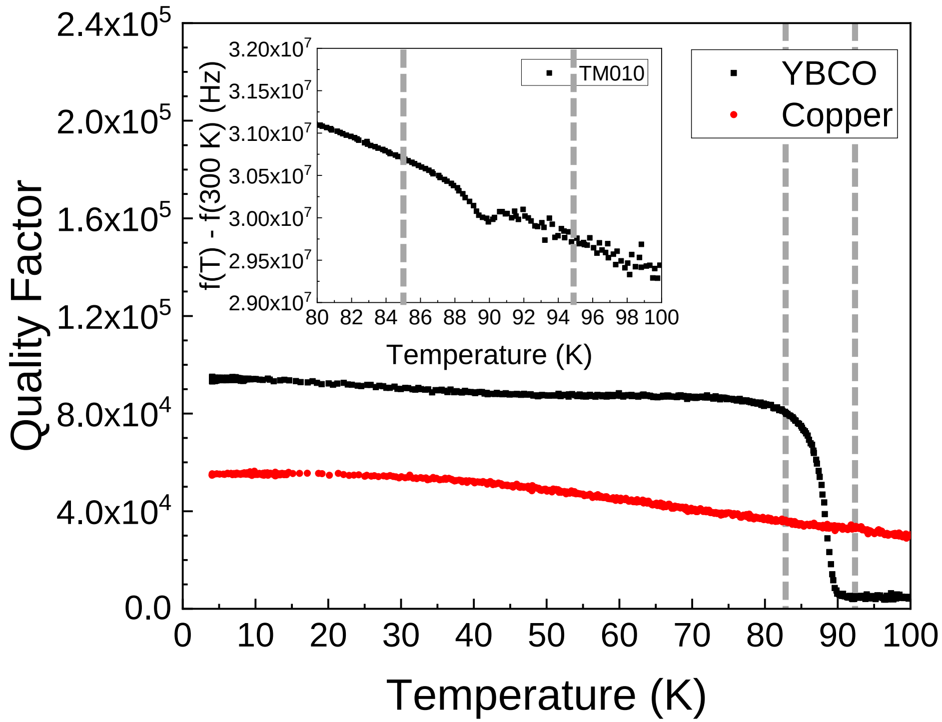

- Normal-superconductor phase transition temperature: 90 K
- Anomalous resonance frequency drop at 90 K: Diverging penetration depth
- Q factor of YBCO at 4 K is 95,000.
- Q factor of oxygen-free high thermal conductivity copper at 4 K is 56,500.

Temperature Measurement Result

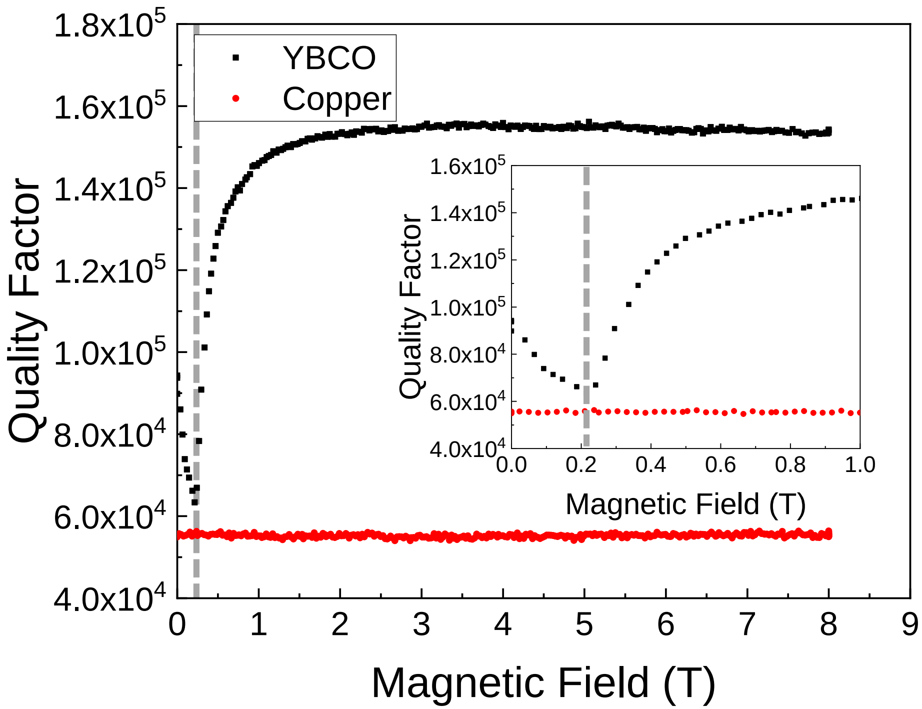

$$\frac{1}{Q} = \sum \frac{P_{YBCO\ film} + P_{etc}}{\omega U_{tot}}$$

- Q factor droped until 0.23 T. (Q ~ 60,000)
- Q factor rose up to the maximum value of 155,000 at around 3.5 T.
- Vortex state transition from vortex liquid to vortex lattice.
- Other source of energy loss could be reduced at the high magnetic field.

Discussion

- The ratio between the known surface resistance of 4 K YBCO (0.02 mOhm) and copper (5 mOhm) at 5-6 GHz is 250.

- The maximum Q factor can be increased with techniques of exposing bare YBCO surface from a tape and eventually reducing the area where surface loss occurs inside the cavity.

Conclusion

- High quality factor superconducting cavities are needed in various high energy physics experiments.
- YBCO has many strength to realize it in GHz range. (Vortex pinning, Well-textured film etc)
- We made